A System for Real-Time Measurement of the Brachial Artery Diameter in *B*-Mode Ultrasound Images

Vincenzo Gemignani*, Francesco Faita, Lorenzo Ghiadoni, Elisa Poggianti, and Marcello Demi

***Abstract*—The measurement of the brachial artery diameter is frequently used in clinical studies for evaluating the flow-mediated dilation and, in conjunction with the blood pressure value, for assessing arterial stiffness. This paper presents a system for computing the brachial artery diameter in real-time by analyzing *B*-mode ultrasound images. The method is based on a robust edge detection algorithm which is used to automatically locate the two walls of the vessel. The measure of the diameter is obtained with subpixel precision and with a temporal resolution of 25 samples/s, so that the small dilations induced by the cardiac cycle can also be retrieved. The algorithm is implemented on a standalone video processing board which acquires the analog video signal from the ultrasound equipment. Results are shown in real-time on a graphical user interface. The system was tested both on synthetic ultrasound images and in clinical studies of flow-mediated dilation. Accuracy, robustness, and intra/inter observer variability of the method were evaluated.**

***Index Terms*—Brachial artery, flow-mediated dilation, real-time systems, ultrasound.**

I. Introduction

SYSTEMS for the measurement of the brachial artery diameter are assuming considerable importance in cardiovascular medicine. The main interest is generated by the assessment of the endothelium-dependent flow mediated dilation (FMD) [1], [2]. The examination, which is based on ultrasound imaging, consists in the measurement of the brachial artery diameter at rest and after reactive hyperemia induced by ischemia of the forearm. An impaired FMD response has been related to cardiovascular risk factors such as smoking [3], [4], hypercholesterolemia [5], [6], hypertension [7], [8], diabetes [9], [10], and hyperhomocysteinemia [11]. The technique is attractive because it is noninvasive, well tolerated, and reproducible [12], so it has been used in a variety of studies. The measurement of the brachial artery diameter is also of interest when assessing changes in the cross-sectional area of the lumen during the cardiac cycle. This measure can be related to pressure waveform [13] and used to evaluate other parameters of high clinical interest, such as distensibility and compliance, which are used to identify vascular changes related to arteriosclerosis [14], [15].

The first studies on the brachial artery were carried out by way of manual analysis on *B*-mode ultrasound images, where the borders of the vessel were identified by means of electronic calipers. The mean between at least three measurements on a single image was commonly used to reduce variability. However, manual analysis showed evident disadvantages as it is a time consuming technique which can lack accuracy and objectivity, so that automations of the measurement were proposed. Most of the methods for automatic or semiautomatic quantification of the FMD were based on offline analysis of *B*-mode ultrasound images, which were recorded by a video cassette recorder (VCR) or stored in a workstation [16]–[20]. In [21], a method for online analysis based on artificial neural networks was presented, which was used to measure the diameter of the artery in real-time during FMD examinations. The paper shows how the method was also able to recover the small dilation during the cardiac cycle, where, however, an average measure over several cardiac events was necessary to quantify this value. An online analysis with high spatial resolution was obtained only in papers where the radio-frequency (RF) signal was analyzed, which is the technique most frequently used to retrieve the diameter waveform [22]–[24]. This approach usually requires special equipment since standard cardiovascular ultrasound systems do not make RF signals available. Furthermore, the presence of the *B*-mode image is nevertheless required to locate the artery exactly and is of great help during the examination to maintain the correct position.

The availability of results in real-time is of particular importance in FMD studies. In these examinations, the quality of the image is a critical component that can compromise the success of the measurement [2]. Indeed, a proper image must be maintained for several minutes to best quantify the transitory response induced by the endothelium. For this reason, adjustments of the position of the probe may be required during the examination, especially to compensate small movements of the patient. The sonographer is largely helped in this task by an immediate feedback from the measurement system. Another advantage of online analysis is the absence of those drawbacks associated with video storing. Recording the video by a VCR means a reduction of the image quality, while an acquisition on a PC requires a large amount of memory. Finally, a real-time examination is obviously less time consuming and this is also an important aspect in clinical applications.

Manuscript received June 29, 2006; revised December 5, 2006. This work was supported in part by the Esaote S.p.A. under Grant IFC_ESAOTE-2003-2004. *Asterisk indicates corresponding author.*

*V. Gemignani is with the Institute of Clinical Physiology, National Research Council, Pisa, 56124 Italy (e-mail: gemi@ifc.cnr.it).

F. Faita and E. Poggianti are with the Institute of Clinical Physiology, National Research Council, Pisa, 56124 Italy.

L. Ghiadoni is with the Department of Internal Medicine, University of Pisa, Pisa, 56126 Italy.

M. Demi is with Esaote S.p.A, Genova, 16153 ITALY. He is also with the Institute of Clinical Physiology, National Research Council, Pisa, 56124 Italy.

Digital Object Identifier 10.1109/TMI.2006.891477

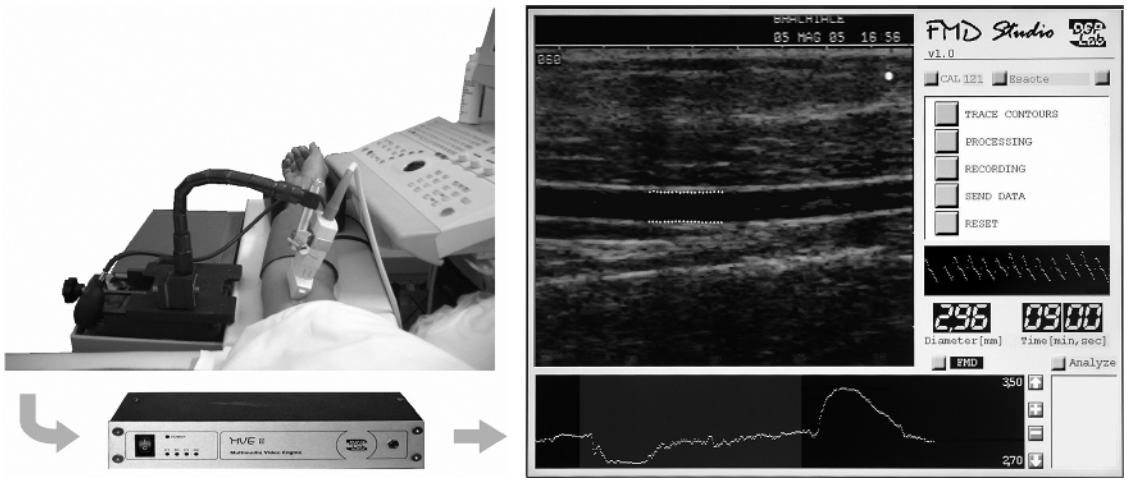

Fig. 1. Experimental setup: the mechanical probe holder, the video processing device, and the GUI are shown.

The system we present in this paper is able to compute the brachial artery diameter in real-time with a temporal resolution of 25 samples/s. This result is obtained by processing the *B*-mode images acquired by the video signal which is usually available in every ultrasound system, so no special ultrasound equipment is required. The method we adopted is based on a fast and robust edge detector, which is used to locate the two borders of the artery. The distance between these borders furnishes the measure of the diameter, which is obtained with the precision necessary to retrieve the small variation induced by the cardiac cycle. The system was tested on synthetic ultrasound images and in *in vivo* FMD examinations.

II. Method

The method is based on a contour tracking technique applied to *B*-mode images of a longitudinal section of the vessel. Detecting the borders of the vessel may prove to be difficult because of the limited quality of the images and because of the presence of speckle noise. We approached the problem by using a new robust edge detector which, in a previous work [25], [26], proved to be also suitable for real-time implementations. This mathematical operator was used in a contour tracking algorithm which was especially designed for the brachial artery. Since the shift of the artery wall is only a few pixels, a temporal filter was added to constrain the movement of the contours. Moreover, the algorithm was modified with some ad hoc adjustments so as to exploit some peculiarities of the images under investigation.

The algorithm was implemented on a standalone video processing device based on a digital signal processing (DSP) board. The device acquires the analog video signal from an ultrasound system and shows the results on a graphical user interface (GUI). A mouse and a keyboard are available to operate the device. The procedure must be initialized by manually tracing two approximated starting borders, an operation that also defines the region of interest (ROI) where the diameter will be computed. This operation is carried out in a GUI window where the ultrasound images are displayed in real-time. The elaboration starts immediately afterwards. The value of the diameter is shown by a numerical display and is plotted on two graphs: the first graph shows the instantaneous measure over a time scale of 5 s; the second graph shows the mean value of the diameter computed over 2 s and displayed over a time scale of 9 min (Fig. 1).

Once initialized, the system does not require any other intervention by the sonographer, who will direct his/her efforts towards maintaining a consistent image throughout the entire examination. In order to make this task easier, a mechanical probe holder, which is similar to those used by [17], was adopted. The device is composed of a jointed arm positioned on a slide which allows micrometric movements of the probe in the direction which is perpendicular to the artery, as we found this to be the most important adjustment necessary to refocus the image.

A. Edge Detector

The edge detector we used is named "mass center of the gray level variability." A detailed description of the mathematical operator and the analysis of its performances in a generic task of real-time contour tracking can be found in [25]. In this paper, we review just some of its characteristics, which are useful to describe the algorithm we developed for the brachial artery.

The mass center of the gray level variability is a vectorial operator defined as follows. Let $f(n,m)$ be the gray level map of an image and let Θ_1 and Θ_2 be two circular domains with radii r_1 and r_2 defined as

$$\Theta \mathrm{i} = \left\{(k,l) \in Z^2 : \sqrt{k^2+l^2} \leq r_i\right\} \quad i = 1,2 \qquad (1)$$

where Z represents the integer numbers and (k,l) are the coordinates of a generic pixel with respect to a Cartesian plane with origin in $\mathbf{p} \equiv (n,m)$. The sizes of the two domains are chosen so that $\Theta_1 \subseteq \Theta_2$, that is $r_1 \leq r_2$. Let us compute the mean value of $f(\mathbf{p})$ on the circular domain Θ_1

$$f_1(\mathbf{p}) = \sum \sum_{(k,l)\in\Theta 1} f(n-k, m-l) w(k,l,r_1) \qquad (2)$$

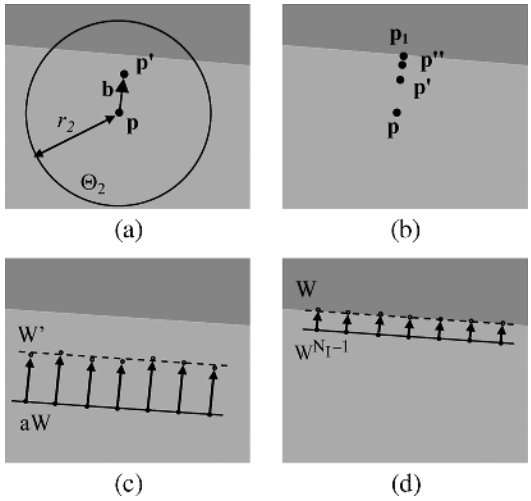

Fig. 2. (a) The $\mathbf{b}$ vector computed at the point $\mathbf{p}$ is perpendicular to the discontinuity and locates a new point $\mathbf{p}'$ which is closer to the discontinuity than $\mathbf{p}$. (b) The nearest point $\mathbf{p_1}$ of the discontinuity can be located by iteratively computing $\mathbf{b}$. (c) Vector $\mathbf{b}$ is computed at $\mathrm{N_P}$ equidistant points of the approximated contour aW so as to obtain a new set of $\mathrm{N_P}$ points which are closer to the border. A new contour W' is obtained by the linear regression of the new set of points. (d) The algorithm is repeated iteratively until the solution converges to the discontinuity W.

where $w(k,l,r_1)$ is a normalized Gaussian weight function with standard deviation equal to $r_1/3$. Let us now associate every pixel of the circular domain Θ_2 to a mass $h(\mathbf{p},k,l)$ so that

$$h(\mathbf{p},k,l)=|f_1(\mathbf{p})-f(n-k,m-l)|\,w(k,l,r_2) \quad (k,l)\in\Theta_2 \tag{3}$$

where $w(k,l,r_2)$ is a normalized Gaussian weight function with standard deviation equal to $r_2/3$. The function $h(\mathbf{p},k,l)$ represents the spatial distribution of the "variability of the gray levels" of the domain Θ_2 with respect to the local mean $f_1(\mathbf{p})$ computed at point $\mathbf{p}$. In other words, the function measures how much the gray level of a point in Θ_2 differs from the local mean value $f_1(\mathbf{p})$ computed in the domain Θ_1.

Let us now compute the mass center of the function $h(\mathbf{p},k,l)$ as

$$\mathbf{b}(\mathbf{p})=\begin{cases}\dfrac{\sum\limits_{(k,l)\in\Theta 2}\sum h(\mathbf{p},k,l)\boldsymbol{\Gamma}}{\sum\limits_{(k,l)\in\Theta 2}\sum h(\mathbf{p},k,l)} & if \quad \sum\limits_{(k,l)\in\Theta 2}\sum h(\mathbf{p},k,l)\neq 0\\ 0 & if \quad \sum\limits_{(k,l)\in\Theta 2}\sum h(\mathbf{p},k,l)=0\end{cases} \tag{4}$$

where $\boldsymbol{\Gamma}$ is a discrete vector with components $(-k,-l)$. In this way, vector $\mathbf{b}$ joins point $\mathbf{p}$ to the mass center $\mathbf{p}'$ of the variability of the gray levels of the domain Θ_2.

When computed at a point $\mathbf{p}$ in the neighborhood of a discontinuity between the gray levels of an image, (4) gives a vector $\mathbf{b}$ that has two important properties Fig. 2(a): 1) $\mathbf{b}$ is perpendicular to the discontinuity; 2) $\mathbf{b}$ applied to $\mathbf{p}$ locates a new point $\mathbf{p}'$ which is closer to the discontinuity than $\mathbf{p}$, independently of the distance from $\mathbf{p}$ and the discontinuity.

According to these properties, when a starting point $\mathbf{p}$ is given, the nearest point $\mathbf{p_1}$ of the discontinuity can be located by iteratively computing the mass center of the gray level variability. When any new iteration occurs, the starting point is the mass center which is determined by means of the previous iteration Fig. 2(b). It is worth noting that the algorithm converges only if the size r_2 of the domain Θ_2 is greater than the distance between $\mathbf{p}$ and the discontinuity.

B. Contour Tracking Algorithm

The contour tracking algorithm is based on the assumption that the segment of the vessel under investigation can be correctly approximated with a cylinder. If we look at the geometry of the brachial artery, we find that this statement is reasonably true for segments of the vessel which are 1–2 cm in length.

With this assumption, the two borders of the longitudinal section of the vessel are approximated by two straight segments. For each of the two borders, let us suppose the starting point to be an approximated contour aW which is a segment in the neighborhood of the discontinuity. We will use vector $\mathbf{b}$ to converge from points of aW to points of the searched for border W. The algorithm consists of the following steps [Fig. 2(c) and (d)].

1) Vector $\mathbf{b}$ is computed at N_P equidistant points of the approximated contour aW so that a new set of N_P points, which are closer to the border W, is obtained.
2) The linear regression of the new set of points is computed, thus obtaining a new contour W' which better approximates the searched for border.
3) Steps one and two are repeated N_I times, until the contour converges to a solution.

Experimentally, we found that the algorithm converges very quickly, with a number of steps that is less than 5, so that we set $N_I=5$ to be the maximum number of iterations.

This algorithm can easily be extended to the whole video sequence, where the approximated contour at the nth frame is the contour computed at the $(n-1)$th frame. In this way, once we have the approximated borders on the first image of the sequence, we can automatically locate the borders throughout the whole sequence.

FMD sequences frequently contain some bad quality images resulting from small movements of the patient. In such images, the algorithm can converge to a completely wrong border and the error can propagate in the subsequent images, causing the algorithm to start from wrong approximated contours. As we previously stated, there is very little movement of the brachial walls during the FMD study and, consequently, the position of the approximated contour should not vary quickly. This assumption can be used to improve the robustness of the contour tracking algorithm where, rather than only use the contour obtained on the previous frame, the approximated contour is computed as the mean position of the N_C contours obtained on the frames $(n-N_C)$th to $(n-1)$th.

A larger value for N_C provides a more robust mechanism. However, a large temporal filtering can lead to failures when the position of the artery walls really changes in the space of a few images. This happens, for example, when the artery dilates and when the cuff is inflated or deflated. Experimentally, we found that an acceptable value is $N_C=75$.

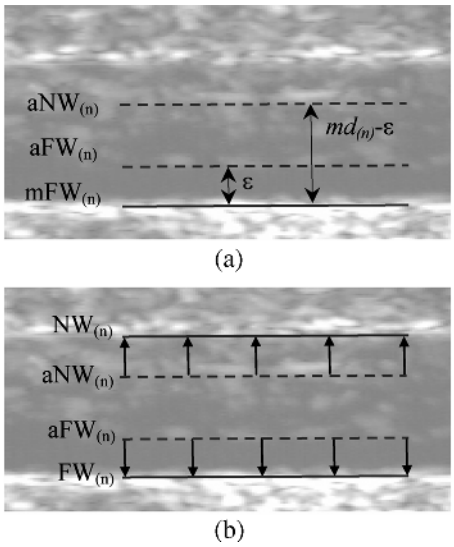

Fig. 3. (a) The approximated far wall $\mathrm{aFW}_{(n)}$ is the segment parallel to $\mathrm{mFW}_{(n)}$ (mean position of the far walls computed on the previous N_C frames) at a distance ε towards the inner part of the vessel. The approximated near wall $\mathrm{aNW}_{(n)}$ is the segment parallel to $\mathrm{mFW}_{(n)}$ at a distance $\mathrm{md}_{(n)}-\varepsilon$, where $\mathrm{md}_{(n)}$ is the mean value of the diameters calculated on the previous N_C images. (b) $\mathrm{NW}_{(n)}$ and $\mathrm{FW}_{(n)}$ are computed by starting from $\mathrm{aNW}_{(n)}$ and $\mathrm{aFW}_{(n)}$, respectively.

C. Aspects Related to Ultrasound

The algorithm described so far was further modified so as to take into account two peculiarities of brachial ultrasound images, which can be used to improve the robustness of the procedure. The first one is that the two borders of the vessel are not of the same quality. The near wall (NW), that is the border which is closer to the probe, is generally less defined than the far wall (FW) because large trailing echoes from the adventitia extend into the media and the intima [27]. Due to this characteristic of the images, the FW can be located more easily and more accurately than the NW, so that we used the former as a reference point for computing the latter. The other feature we exploited is that the area which is internal to the vessel is less noisy than the external area. This difference is due to the presence of blood, which generates weak echoes. The presence of a region with less noise is advantageously exploited by the edge detection algorithm. This is obtained simply by forcing the algorithm to locate the two borders by starting from the internal part of the vessel.

These two peculiarities were used to modify the way the two approximated contours were obtained. As for the FW, we used a simple variation of the algorithm described so far where, once the mean position $\mathrm{mFW}_{(n)}$ of the previous N_C contours is computed, the approximated contour $\mathrm{aFW}_{(n)}$ is the segment parallel to $\mathrm{mFW}_{(n)}$ at a distance ε towards the inner part of the vessel (Fig. 3). In this way, the assessment of the current contour $\mathrm{FW}_{(n)}$ began from points in the inner region of the vessel, where the noise is less. As regards the NW, since the quality of this discontinuity is worse than that of the FW, we also computed the approximated contour $\mathrm{aNW}_{(n)}$ by starting from $\mathrm{mFW}_{(n)}$. Let $\mathrm{md}_{(n)}$ be the mean value of the diameters calculated on the previous N_C images, then $\mathrm{aNW}_{(n)}$ was obtained as the parallel to $\mathrm{mFW}_{(n)}$ at a distance $\mathrm{md}_{(n)}-\varepsilon$.

D. The Final Algorithm

To summarize, for the nth image of the sequence, the contour tracking algorithm consists of the following steps.

1) *Retrieval of information from previous images*. The mean position mFW(n) of the far walls obtained in the previous N_C frames and the mean value $\mathrm{md}_{(n)}$ of the diameters obtained in the previous N_C frames are computed.
2) *Contour approximation*. The approximated contour $\mathrm{aFW}_{(n)}$ is computed as the segment parallel to $\mathrm{mFW}_{(n)}$ at a distance ε towards the inner part of the vessel. The approximated contour $\mathrm{aNW}_{(n)}$ is computed as the segment parallel to $\mathrm{mFW}_{(n)}$ at a distance $\mathrm{md}_{(n)}-\varepsilon$ towards the inner part of the vessel.
3) *Contour and diameter computation*. The contour $\mathrm{FW}_{(n)}$ and the contour $\mathrm{NW}_{(n)}$ are obtained by starting from $\mathrm{aFW}_{(n)}$ and $\mathrm{aNW}_{(n)}$, respectively, then the diameter is computed.

The diameter is computed by starting from the two final borders which, in theory, should be parallel. In practice, however, this hypothesis is not exactly true and an approximation must be introduced. Since we assumed that the FW is better estimated than the NW, the FW is taken as the reference line and the diameter is computed as the mean value of the distances between points of the NW and the line FW. More efficiently, the diameter is computed as the distance between the central point of the segment NW and the line FW.

The whole algorithm must be initialized with a starting border FW and a starting value for the diameter of the vessel. The sonographer provides this information by manually tracing two approximated borders before the procedure is started, an operation that does not require particular precision. The starting diameter is obtained by calculating the distance between these two borders.

In FMD examinations, the initialization of the contours should be carried out only once, before taking the baseline measurement. However, a reinitialization may be required during the exam, when the contour tracking algorithm converges to a wrong solution. A typical example is when one of the two contours converges to a wrong border, usually outside the vessel. In these cases, the sonographer can drag this contour to the correct position and the algorithm automatically restarts without changes in the ROI. When more severe failures occur, contours can be entirely retraced.

E. Implementation Overview

A stand-alone video processing board [28] was used for the real-time analysis. The main component (Fig. 4) is the Texas Instruments' TMS32C6415, a high performance digital signal processor particularly suited for computationally intensive video processing applications. The board contains an analog video decoder, which can acquire the video signal generated by the ultrasound equipment, and a VGA video output, which is used for the GUI. A USB port is available to connect the mouse and keyboard, and an Ethernet port permits communication with a remote workstation.

The architecture of the system is not very different from that of a small PC equipped with a frame grabber, as both the sys-

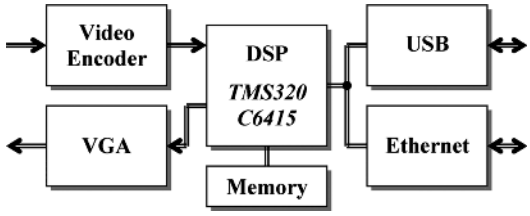

Fig. 4. Architecture of the DSP video processing system.

tems are based on a programmable processor and have similar peripherals. The complexity of our device is lower than that of a PC, as our system was not designed for general-purpose applications. However, its processing power is remarkably higher and the real-time execution of the code is ensured by a special operating system. In addition, a software framework is already available for the development of video processing applications. This software, which was developed for simplifying the use of the system, manages video data flow, the GUI and all the peripherals present in the system.

The above described algorithm was implemented in optimized C language and was integrated in the framework. The computation of the edge detector (4) is the part of the algorithm which most affects the elaboration time since it has to be carried out several times. When for each of the two contours $\mathbf{b}$ is computed at $N_P = 20$ points and when the worst case is considered, i.e., where the contour tracking algorithm converges in five steps, the computation of the edge detector is repeated 200 times. However, the execution of this type of algorithm in the TMS32C6415 is very fast because the processor is optimized for both multiply-and-accumulate operations and for absolute value of difference operations [29]. In the end, the real-time performance was achieved without great difficulty as the overall CPU load turned out to be 13%.

III. Experimentation

The method was initially tested on sequences of synthetic ultrasound images. The aim of the simulation, which was carried out offline by using a PC, was to estimate the accuracy and precision of the algorithm in assessing the diameter. Subsequently, the method was tested in *in vivo* studies of flow mediated dilation and the agreement with a manual gold standard, the intra/inter observer variability and the robustness of the technique were evaluated. Finally, a comparison with another automatic measurement method was reported.

A. Synthetic Images

Synthetic images of the brachial artery were obtained by using the ultrasound simulation program Field II [30]. A three-dimensional phantom was made, where the brachial artery was modeled as a cylinder which was positioned parallel to the probe at a distance z_0 from the surface of the probe itself Fig. 5(a). 100 000 scatterers were randomly distributed within the volume of the phantom and strong scatterers were placed to simulate boundaries [31]. This setup was used to generate a sequence of images that reproduces the small vasodilations due to the cardiac cycle. The changes of diameter (ranging from

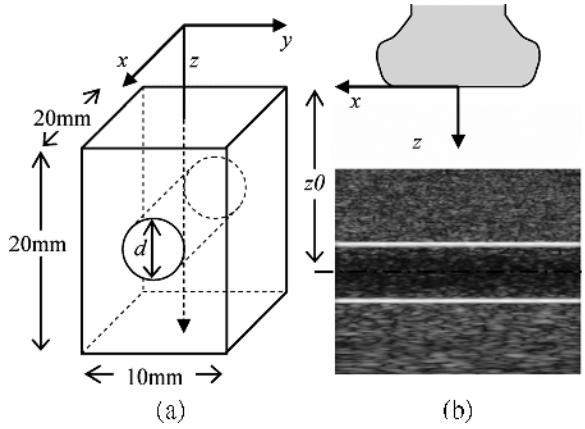

Fig. 5. (a) Geometry of the phantom used to generate synthetic images of the brachial artery. (b) Example of a synthetic image of the brachial artery obtained by Field II.

3.9 mm to 4.0 mm) were obtained by moving all the scatterers in the radial direction with respect to the axis of the artery. A slow movement in the z direction from $z_0 = 20.0$ mm to $z_0 = 20.3$ mm was also added to simulate a variation in the vertical position of the probe.

Scans were made by simulating a 13 MHz linear array vascular probe with 192 elements. The images we obtained were *B*-mode 256 gray levels images with a resolution of 13 pixels/mm Fig. 5(b). A sequence of 100 images was synthesized, which simulates five cardiac cycles. The diameter d_i in the ith image is

$$d_i = d_0 + \Delta d_i \quad i = 1 \ldots 100 \tag{5}$$

where $d_0 = 50.7$ pixels (3.9 mm) and $0 < \Delta d_i < 1.3$ pixels.

The sequence was analyzed both manually and automatically by an expert. The manual measurement was carried out by using a software utility developed in Matlab, which implemented an algorithm similar to that used in automatic analysis: the sonographer had to manually locate ten points on both the near and the far wall, then the two borders of the vessel were obtained by the linear regression of the two sets of points. In the automatic measurement, the expert had only to trace the starting contour on the first frame of the sequence, then the diameter was computed without human intervention in all the subsequent images.

B. Brachial Images

The method was tested on a total of 270 FMD examinations, taken from three clinical studies. The subjects were 48% F 52% M, their age varied between 18 and 76 years and the body mass index was between 20 and 34 $\mathrm{Kg/m^2}$. 18% of the patients were healthy subjects, 16% were affected by coronary disease, 53% had cardiovascular risk factors, and 13% had other pathologies which were not related to cardiovascular risks. The data-set covers a wide range of brachial artery diameters, responses to FMD and image quality (Fig. 6).

All the scans were carried out by an experienced vascular sonographer and were analyzed online. In order to allow a repetition of the measurements, the sequences were also recorded

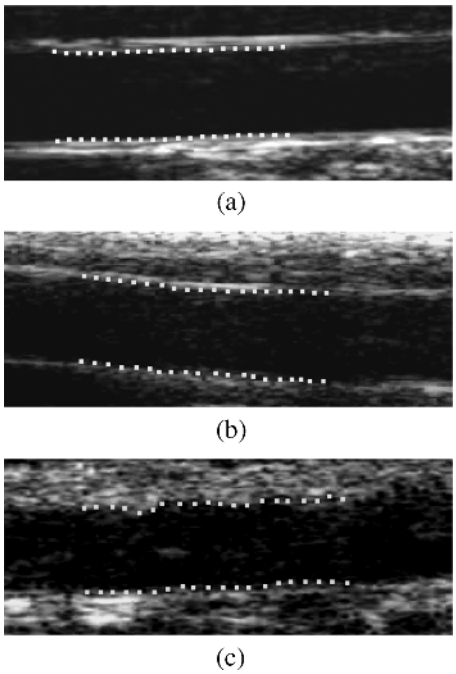

Fig. 6. Result of automatic analysis on three images of different quality. (a) High quality—the walls of the vessel are clearly visible and well defined. (b) Medium quality—the walls of the vessel are clearly visible but they are not well defined. (c) Poor quality—the walls of the vessel are not clearly visible and echoes may be present within the vessel.

on a PC with an image resolution of 768 × 576 pixels and rate of 1 frame/second.

Vascular ultrasound scans were performed with subjects supine, at rest, in a quiet air conditioned room (22°C–24°C). A *B*-mode scan of the right brachial artery was obtained in longitudinal section between 5 cm and 10 cm above the elbow using a 13.0 MHz linear array transducer and a high resolution ultrasound system (ESAOTE SpA Technos MPX and MyLab 25). The ECG trigger was used to obtain end-diastolic images. Following a 1 min measurement of the baseline diameter, a cuff (placed around the forearm just below the elbow) was inflated for 5 min at 200 mmHg and then deflated to induce reactive hyperemia. The diameter of the artery was then measured for 3 min and the FMD was calculated as the percent increase with respect to the baseline.

The set of FMD sequences was used to test the performance of the proposed method. A comparison with manual gold-standard analysis was made on a set of 160 images which were extracted from twenty FMD sequences. Eight images were extracted from each sequence: four in the baseline; four in the post occlusion phase at 60, 90, 120, and 150 s after the cuff deflation. The dataset was analyzed both manually and automatically by an expert. Both measurements were repeated twice in independent runs and the mean between the two manual measures was assumed to be the gold-standard. The manual analysis was carried out in the same manner as in synthetic images. The automatic measurement required the manual tracing of the contours for each set of image coming from a single sequence. Regression analysis and Bland–Altman plots [32] were used to compare the results.

TABLE I
ERROR ANALYSIS (MEAN ± SD) FOR THE SEQUENCE OF SYNTHETIC IMAGES

	Manual	Automatic
Diameter error	-1.85 ± 0.36 [pixels]	-2.36 ± 0.037 [pixels]
Δd/d0 error	-0.31% ± 0.75%	-0.013% ± 0.069%

The inter/intra-observer variability of the method was tested on four FMD sequences which contained 60 s of baseline and 180 s of acquisition subsequent to the cuff deflation, for a total of 240 images per sequence. The dataset was analyzed by three observers, each of whom repeated the measurement four times in independent runs. The only task the observer had was to place the starting borders, therefore, the position and dimensions of the ROI were what caused the variability in the measure. The coefficient of variation (CV) was calculated to quantify inter/intra-observer variability.

The robustness, that is the capability of providing results without apparent failures, was estimated by a qualitative classification of the set of 270 sequences. The sonographer who carried out the examination made a judgment as to the quality of the results depending on the presence of artifacts in the diameter curve or failures in the contour tracking algorithm.

Finally, a comparison with another automatic method based on the analysis of *B*-mode images was reported. This second method, proposed by Beux *et al.* in [17], had been used at the Department of Internal Medicine of the University of Pisa for six years in clinical trials where a total of more than 1000 patients were examined. The comparison was carried out on 20 FMD sequences that an expert sonographer judged to be also suitable for the analysis by Beux's *et al.* method.

IV. RESULTS

A. Analysis of Synthetic Images

Let $\hat{d}_i$ be the diameter measured in the ith image of the sequence. The error committed in the assessment of the diameter is

$$e_{Di} = \hat{d}_i - d_i. \tag{6}$$

The mean and the standard deviation (SD) of this error for both the manual and the automatic analysis are reported in the first row of Table I. Results show that both measurements of the diameter have a significant bias. The cause of this error can be understood by looking at how the image is formed by starting from the ultrasound signal. The envelope of the RF signal, in fact, gives rise to smooth edges in correspondence to the borders of the vessel and this shape of the gray level discontinuities provoked the edge detector algorithm to converge at points which are slightly shifted towards the internal region of the vessel. Manual measurements were affected by a similar error as in this case also the expert was looking for a gray level discontinuity.

The presence of a bias in the measure of the diameter is not a problem in the assessment of absolute diameter changes ($\Delta d_i = d_i - d_0$). On the contrary, this bias may be relevant when the diameter value is used to compute relative diameter

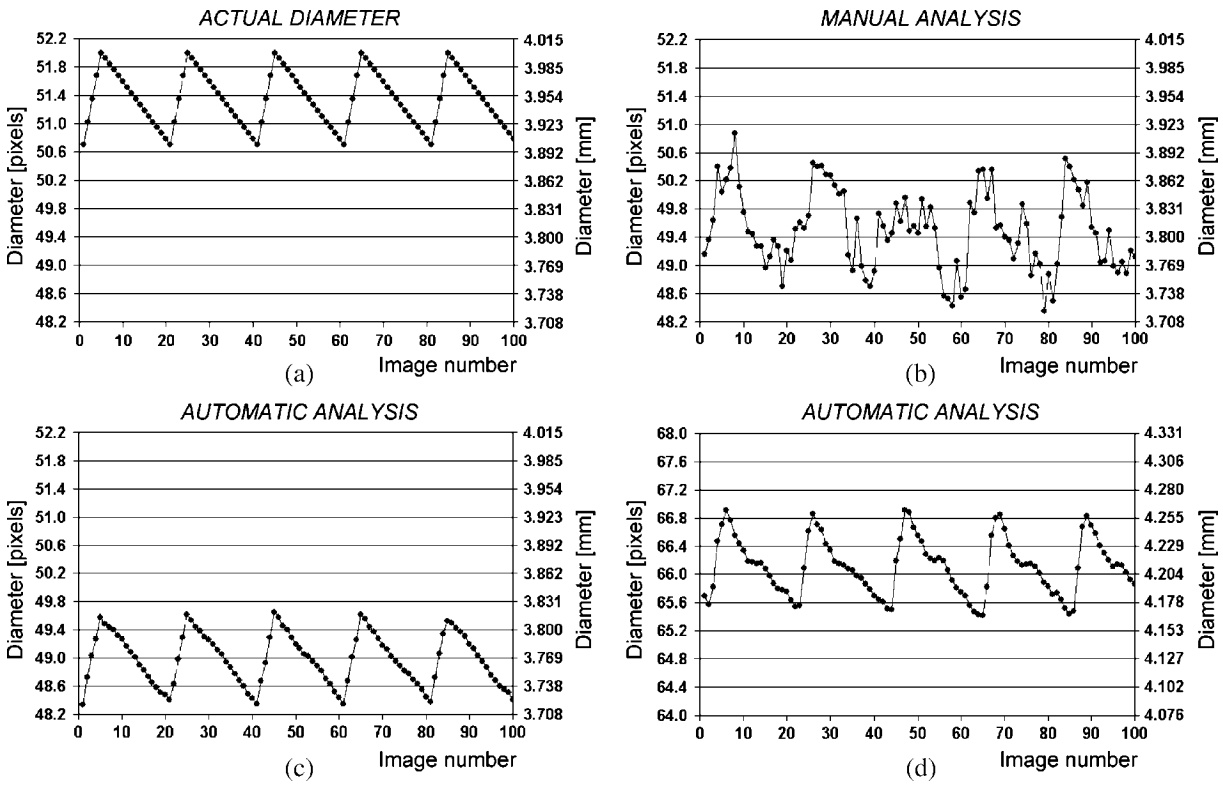

Fig. 7. Actual diameter (a) in the sequence of synthetic images and results of (b) manual analysis and (c) automatic analysis. (d) Diameter over five cardiac cycles computed by automatic analysis on *in vivo* images. The plot qualitatively confirms the results of the simulation.

changes $(\Delta d_i/d_0)$, such as in FMD examinations. This error can be quantified as follows.

Let $aFMD$ be the value computed from unbiased diameter measures

$$\mathrm{aFMD} = \frac{d - d_0}{d_0}. \tag{7}$$

Let us consider a diameter measure $\hat{d}$ with a bias $\overline{e}_D$, that is $\hat{d} = d + \overline{e}_D$. The error $\mathrm{e_{FMD}}$ we commit when computing the FMD from biased diameter measures is

$$e_{\mathrm{FMD}} = \frac{\hat{d} - \hat{d}_0}{\hat{d}_0} - \frac{d - d_0}{d_0} = -\frac{\overline{e}_D}{d_0 + \overline{e}_D} \cdot \mathrm{aFMD}. \tag{8}$$

In our experimental condition, we had $d_0 = 50.7$ pixels and the mean error $\overline{e}_D$ is -1.85 pixels for manual measurements and -2.36 pixels for automatic measurements. These values in (8) give $e_{\mathrm{FMD}} = 0.035 \cdot \mathrm{aFMD}$ and $e_{\mathrm{FMD}} = 0.044 \cdot \mathrm{aFMD}$ respectively, which are acceptable errors for this sort of examination.

The second row of Table I reports mean and SD of the error we committed in the assessment of the relative diameter change $\Delta d_i/d_0$. In this case, the value d_0 was obtained as the mean value of the diameters computed at images 1, 21, 41, 61, 81, where $\Delta d_i = 0$. Results confirm the precision of automatic analysis.

Having found that the mean values of the error were of the same extent, it must be stated that, on the contrary, the SD was considerably lower in automatic analysis, which was, therefore, able to retrieve the absolute diameter change with greater precision. This result is also evident if we compare the curve of the actual diameter Fig. 7(a) with the curves obtained by manual analysis Fig. 7(b) and automatic analysis Fig. 7(c), respectively.

Analogous results were obtained in tests carried out on *in vivo* images with experimental conditions similar to those of the simulation: 13 MHz linear array probe and an image resolution of 15.7 pixel/mm. Results may be affected by a bias (we did not have a "true" measure of the brachial artery that confirmed this statement) but a subpixel precision of the measure was clearly obtained as the curve of the diameter change during the cardiac cycle is correctly traced even when the difference between maximum and minimum is in the order of one pixel in size Fig. 7(d).

This experimentation was also used to set the parameters of the edge detector. Larger domains Θ_2 provided more robust but less accurate measures. The configuration we chose for the analysis was $r_1 = 6$ pixels and $r_2 = 12$ pixels and the number of points at which the edge detector is computed in each border was $N_P = 20$.

B. Analysis of Brachial Images

1) Comparison With Manual Analysis: The agreement between automatic and manual analysis was evaluated both in terms of diameter and of %FMD. The latter was evaluated in the post occlusion phases only, where the baseline diameter was computed as the mean value between the four baseline measures. Results of regression analysis are shown in Fig. 8: slope and intercept were not significantly different from 1 and 0, respectively, for both measures. Fig. 9 shows the Bland–Altman plots comparing automatic and gold-standard measurements. The measure of the diameter has a bias of -0.60 pixels (95% CI from -0.47 to -0.72 pixels), which confirms the results we

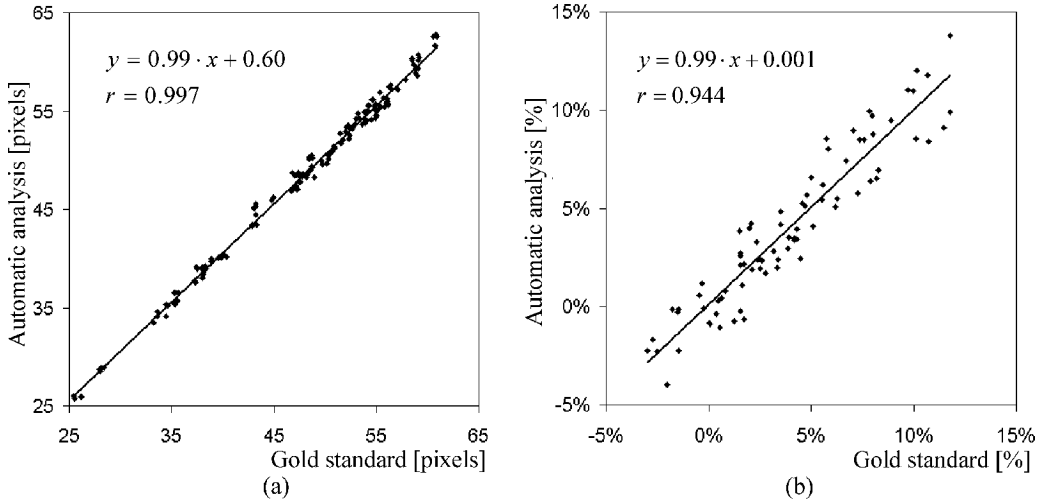

Fig. 8. Regression analysis of our method versus gold standard in terms of (a) diameter and (b) %FMD.

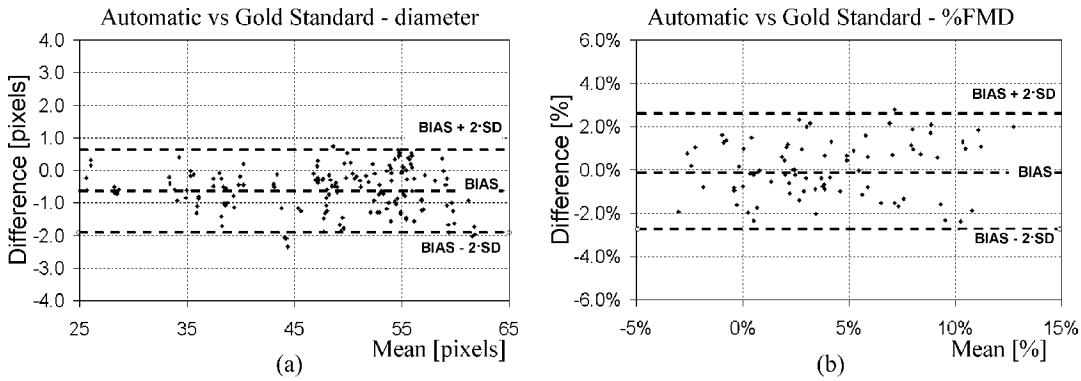

Fig. 9. Bland–Altman plot of our method versus the gold standard in terms of (a) diameter and (b) %FMD.

found in synthetic images where the difference in the bias levels was -0.51 pixels. The SD of the differences was 0.68 pixels. In terms of %FMD, the bias between the two measurements was negligible (0.07% with 95% CI from -0.22% to 0.36%) and the SD of the difference was within acceptable error limits for this sort of examination (1.31%).

The repeatability of the two measurements was analyzed by Bland–Altman plots comparing the two manual sessions [Fig. 10(a) and (b)] and the two automatic sessions [Fig. 10(c) and (d)]. In both cases, the bias is not significantly different from zero whereas the SD of the difference is greater in the manual analysis ($\mathrm{SD} = 0.71$ pixels for the diameter; $\mathrm{SD} = 1.64\%$ for the FMD) than in the automatic analysis ($\mathrm{SD} = 0.21$ pixels for the diameter; $\mathrm{SD} = 0.66\%$ for the FMD).

2) Interobserver and Intraobserver Variability: The results obtained by the three observers were compared both in terms of diameter and of %FMD. The latter was computed in the 180 images of postocclusion with respect to a baseline value computed in the first 60 images.

For a single observer, the CV of the four measurements performed on each image was computed. The mean value and the standard deviation of CV was reported both for the single sequences and for the whole set of images (first three rows of Table II and Table III), and the latter was an evaluation of the intraobserver variability. The CV of the total of twelve measures performed by the three observers on each image was then computed, so as to quantify the interobserver variability (last row of Table II and Table III).

The interobserver variability was affected by the fact that the three observers could choose different ROIs in the image, where the size of the artery was slightly different. These differences, however, were rather small and were negligible when measuring the %FMD. In conclusion, results show how the manual choice of the starting borders does not significantly affect the measurement of both the diameter and the %FMD.

3) Robustness: The results obtained by processing the whole set of 270 sequences were qualitatively classified by an expert sonographer. We considered the sequences where results did not show evident artifacts both in the baseline and in the post occlusion to be *excellent* (10%). In these cases, the maxima vasodilation and the baseline value can be found automatically on the diameter curve. Sequences where the system failed in the computation of the diameter in only a few images were classified as *good* (78%). These are cases where the patient moved and the probe needed to be realigned. The diameter curve showed small artifacts (1–3 s long) in correspondence to these events, which, however, could be easily recognized and manually discarded. In these examinations, possible failures of the contour tracking algorithm were corrected by dragging the

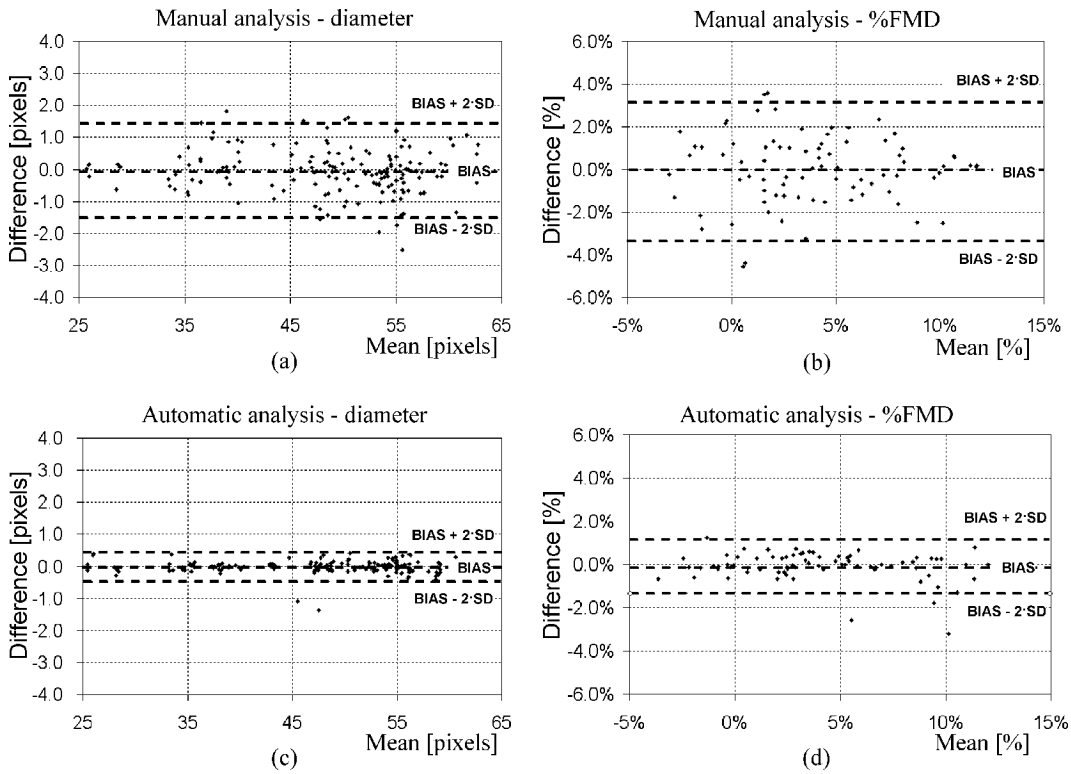

Fig. 10. Bland–Altman plots which compare the two manual measurements [(a) and (b)] and the two automatic measurements [(c) and (d)].

TABLE II
MEAN AND STANDARD DEVIATION OF THE CV FOR THE DIAMETER MEASURE

	Seq. I	Seq. II	Seq. III	Seq. IV	Intra-observer
Observer 1	0.43% ± 0.14%	0.30% ± 0.22%	0.13% ± 0.07%	0.34% ± 0.14%	0.30% ± 0.19%
Observer 2	0.33% ± 0.17%	0.53% ± 0.35%	0.15% ± 0.06%	0.38% ± 0.15%	0.34% ± 0.25%
Observer 3	0.40% ± 0.16%	0.54% ± 0.38%	0.08% ± 0.04%	0.24% ± 0.14%	0.31% ± 0.27%
Inter-observer	0.80% ± 0.17%	0.74% ± 0.33%	0.16% ± 0.14%	0.64% ± 0.19%	

TABLE III
MEAN AND STANDARD DEVIATION OF THE CV FOR THE %FMD MEASURE

	Seq. I	Seq. II	Seq. III	Seq. IV	Intra-observer
Observer 1	0.24% ± 0.12%	0.31% ± 0.22%	0.10% ± 0.05%	0.23% ± 0.13%	0.21% ± 0.16%
Observer 2	0.28% ± 0.14%	0.47% ± 0.35%	0.11% ± 0.06%	0.22% ± 0.10%	0.26% ± 0.23%
Observer 3	0.25% ± 0.13%	0.51% ± 0.37%	0.09% ± 0.05%	0.23% ± 0.11%	0.27% ± 0.25%
Inter-observer	0.31% ± 0.12%	0.56% ± 0.30%	0.14% ± 0.14%	0.30% ± 0.10%	

contour to the correct position. The sequences were classified as *sufficient* (9%) when artifacts were more severe but the diameter curves were however useful to quantify the %FMD. In these examinations, possible failures of the contour tracking algorithm were corrected by retracing the contours. When the examination did not provide any clinical information, the sequence was classified as *poor* (3%).

4) Comparison With a Previous Method: In the comparison between the two automatic methods, all the images in the 60 s of baseline and in the 180 s subsequent to the cuff deflation were processed. The correlation between the two sets of diameter measures is high (0.992) but the regression analysis showed slope and intercept which were significantly different from 1 and 0, respectively Fig. 11(a). This is due to the fact that the two methods compute the diameter of the vessel in a significantly different way. Our method finds the edge of the vessel at the lumen-intima interface while the second finds the edge of the vessel in proximity to the adventitia. The difference is more evident when we analyze the diameter measures by Bland–Altman plot Fig. 12(a): the bias is as great as −12.6 pixels (Beux's *et al.* method provides larger values as it includes the thickness of the tunica) and the SD of the difference is not small either (1.76 pixels). Besides this large bias, a certain lack of agreement in the measure of the diameter can be understood however, if we consider that the SD value is largely affected by the different thickness in the tunica between the various sequences. This can be observed by applying Bland–Altman statistic to the 20 sequences separately (i.e., on the 60 measures of baseline plus the 180 measures subsequent to the cuff deflation of a single sequence). Bias values ranged from −7.7 to −15.1 pixels, while

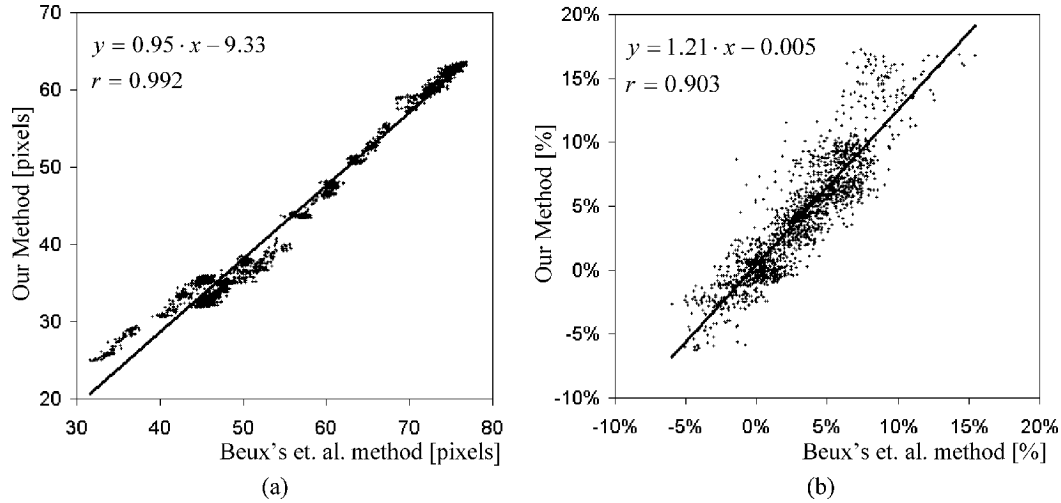

Fig. 11. Regression analysis of our method versus Beux's *et. al.* method in terms of (a) diameter and (b) %FMD.

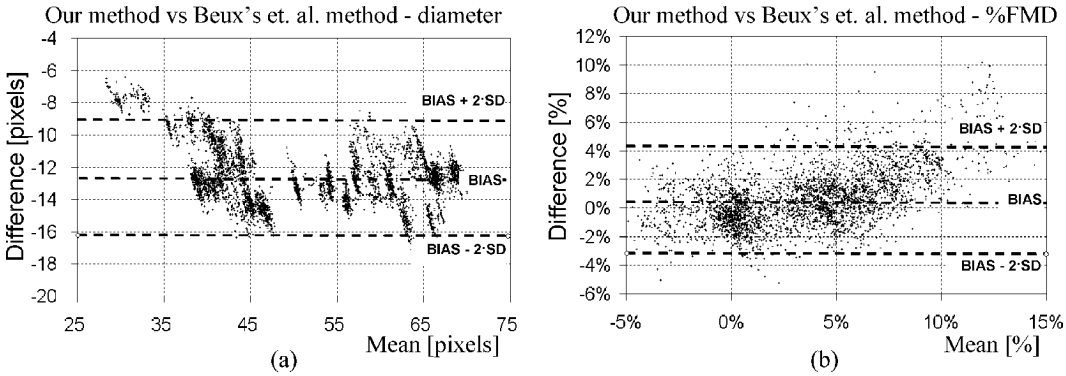

Fig. 12. Bland–Altman plot of our method versus Beux's *et. al.* method in terms of (a) diameter and (b) %FMD.

SDs where significantly lower: the SD ranged from 0.43 to 0.87 pixels, with a mean value of 0.65 pixels.

Regression analysis Fig. 11(b) and Bland–Altman plot Fig. 12(b) comparing %FMD provide similar results.

Despite these observations, it is interesting nonetheless to compare the two methods in terms of robustness, as the oldest one have been successfully used for several years in a large number of clinical studies. For this reason, an expert sonographer analyzed the results provided by the two systems and discharged the images where the algorithms failed. Our method failed in 5% of the 4800 images, while failures were 32% for Beux's *et al.* method. Moreover, while the former was able to provide a significant result for all the sequences, the latter completely failed in two examinations.

V. Conclusion and Discussion

A new method for real-time measurement of the brachial artery diameter has been presented. Tests on synthetic images showed how the new algorithm is able to obtain this measure with high precision, so it can also retrieve the small variations in size which are induced by the cardiac cycle. The method was compared with a manual gold-standard analysis in *in vivo* FMD examinations; the results confirmed the agreement of the two measurements and higher precision and repeatability of the automatic analysis. Tests repeated by three expert sonographers on a set of images showed a low intra/inter observer variability of the method and clinical studies with a total of 270 patients were used to evaluate its robustness. The method was also compared with a previous automatic method based on the analysis of *B*-mode images and the results showed that the robustness of the new method is greater. However, the comparison also highlighted how the two methods provide rather different measures of the diameter and consequently different FMD values.

The difficulty in measuring the brachial artery diameter in *B*-mode ultrasound images is due to a poor definition of the artery walls and to the presence of speckle noise. In this situation, an automatic technique based on edge detection might give unsatisfactory results because of the limits of a local analysis, which is affected by low-level features of the images. A previous paper stressed this issue and proposed a solution based on image registration [20], which is a global analysis strategy. In this paper we faced the problem by means of an edge detector operator which was computed on rather large domains. This choice makes the mathematical operator itself more robust to both the noise and the artifacts due to the poor definition of the discontinuities.

However, the size of the operator does not allow us to make a distinction between lumen-intima boundary (LIB) and media-adventitia boundary (MAB) as the artery wall is seen as a single discontinuity. Our experience suggests that it is very difficult to

obtain a good and reliable automatic distinction between the two boundaries. Indeed, the intima-media thickness of the brachial artery is sometimes so small that the tunica appear almost as a single structure. For these reasons we opted for a more regional approach, which ensured greater robustness and precision of the method. Our edge detector converges to the LIB when the intima tunica is visible, a condition which is desirable because it ensures that the imaging plane is bisecting the vessel [2] and which can be obtained easily enough with modern ultrasound equipment [33]. In the cases where the intima is barely visible or even invisible, the algorithm converges to the MAB. Nonetheless, with the technique we proposed, explicit information on how the diameter will be computed is provided to the sonographer even before the examination is started.

The presence of the intima in only a part of the sequence remains, nonetheless, a source of error. The sonographer must try to prevent the problem by constantly adjusting the position of the probe so as to maintain the consistency of the image, which is the main issue in FMD examinations. This is generally possible, even if sometimes, especially when the LIB is intermittently present, the problem can cause artifacts in the diameter curve. The sonographer must take into account these artifacts when analyzing the diameter curve to compute the %FMD.

Another source of potential error may be a variation in the wall thickness during the examination. However, the extent of this variation [33] is not so great as to suggest that this is a limitation to the technique we adopted. A further potential problem is the presence of bias in the measure of diameter, which is a drawback common to all measurement methods, including manual analysis. We quantified the bias in the experimentation we carried out on synthetic images, where the value of the diameter was known *a priori*. We found that the amount of bias was not such as to lead to significant errors in the computation of the %FMD.

The use of the method in FMD clinical studies highlighted several advantages of real-time analysis. The saving of time and the simplicity of the system, which does not require storing and retrieving of large image sequences, are the more evident. Another important aspect related to the real-time analysis is that the performance of the algorithm can be assessed before the examination is started. This means that the sonographer can optimize the image (even refocus it at a different section of the artery) until the result is satisfactory, and subsequently start the examination. The feedback is also important while the examination is in progress to correct the inevitable movements of the patient. By looking at the borders which are returned by the contour tracking algorithm, the sonographer can easily understand if the measurement is being carried out correctly and can act on the position of the probe when artifacts occur. These aspects of real-time analysis proved to be very important in order to increase the robustness of the examination.

As regards the hardware platform we adopted in this paper, a DSP video board proved to be a very powerful and flexible solution. The implementation of the algorithms was fairly simple and real-time performances were obtained by using only a fraction of the CPU load, leaving space for further developments of the procedure. The hardware device can be easily connected to any ultrasound equipment provided with an analog video output. At present, 15 European research centers are successfully using the method with different ultrasound systems.

The method we propose still requires manual intervention when the contour tracking algorithm fails. In FMD examinations, this is typically due to a movement of the patient which provokes the algorithm to converge to a wrong discontinuity of the image. These errors are corrected while the examination is in progress by repositioning the contour, but the operation could be automated and most of these errors could be prevented by using a motion estimation technique. Nevertheless, a number of examinations carried out in clinical trials show some artifacts in the diameter curve. At present, we manually discharge the points where these artifacts occur, as we found that this operation can be easily carried out by the sonographer once the examination is over. An algorithm for the automatic elimination of these outliers could be added to improve the objectivity of the results.

REFERENCES

[1] D. S. Celermajer, K. E. Sorensen, V. M. Gooch, D. J. Spiegelhalter, O. I. Miller, I. D. Sullivan, J. K. Lloyd, and J. E. Deanfield, "Non-invasive detection of endothelial dysfunction in children and adults at risk of atherosclerosis," *Lancet*, vol. 340, no. 8828, pp. 1111–1115, Nov. 7, 1992.

[2] M. C. Corretti, T. J. Anderson, E. J. Benjamin, D. Celermajer, F. Charbonneau, M. A. Creager, J. Deanfield, H. Drexler, M. Gerhard-Herman, D. Herrington, P. Vallance, J. Vita, and R. Vogel, "Guidelines for the ultrasound assessment of endothelial-dependent flow-mediated vasodilation of the brachial artery: A report of the International Brachial Artery Reactivity Task Force," *J. Amer. Coll. Cardiol.*, vol. 39, no. 2, pp. 257–265, Jan. 16, 2002.

[3] D. S. Celermajer, K. E. Sorensen, D. Georgakopoulos, C. Bull, O. Thomas, J. Robinson, and J. E. Deanfield, "Cigarette smoking is associated with dose-related and potentially reversible impairment of endothelium-dependent dilation in healthy young adults," *Circulation*, vol. 88, no. 5, pt. 1, pp. 2149–2155, Nov. 1993.

[4] M. C. Corretti, G. D. Plotnick, and R. A. Vogel, "Smoking correlates with flow-mediated brachial artery vasoactivity but not cold pressor vasoactivity in men with coronary artery disease," *Int. J. Card. Imag.*, vol. 14, no. 1, pp. 11–17, Feb. 1998.

[5] R. A. Vogel, M. C. Corretti, and G. D. Plotnick, "Changes in flow-mediated brachial artery vasoactivity with lowering of desirable cholesterol levels in healthy middle-aged men," *Amer. J. Cardiol.*, vol. 77, no. 1, pp. 37–40, Jan. 1, 1996.

[6] J. O. Toikka, M. Ahotupa, J. S. Viikari, H. Niinikoski, M. Taskinen, K. Irjala, J. J. Hartiala, and O. T. Raitakari, "Constantly low HDL-cholesterol concentration relates to endothelial dysfunction and increased in vivo LDL-oxidation in healthy young men," *Atherosclerosis*, vol. 147, no. 1, pp. 133–138, Nov. 1, 1999.

[7] J. B. Park, F. Charbonneau, and E. L. Schiffrin, "Correlation of endothelial function in large and small arteries in human essential hypertension," *J. Hypertension*, vol. 19, no. 3, pp. 415–420, Mar. 2001.

[8] L. Ghiadoni, Y. Huang, A. Magagna, S. Buralli, S. Taddei, and A. Salvetti, "Effect of acute blood pressure reduction on endothelial function in the brachial artery of patients with essential hypertension," *J. Hypertension*, vol. 19, no. 3, pt. 2, pp. 547–551, Mar. 2001.

[9] J. Lambert, M. Aarsen, A. J. Donker, and C. D. Stehouwer, "Endothelium-dependent and -independent vasodilation of large arteries in normoalbuminuric insulin-dependent diabetes mellitus," *Arterioscler Thromb Vasc. Biol.*, vol. 16, no. 5, pp. 705–711, May 1996.

[10] H. Kawano, T. Motoyama, O. Hirashima, N. Hirai, Y. Miyao, T. Sakamoto, K. Kugiyama, H. Ogawa, and H. Yasue, "Hyperglycemia rapidly suppresses flow-mediated endothelium-dependent vasodilation of brachial artery," *J. Amer. Coll Cardiol.*, vol. 34, no. 1, pp. 146–154, Jul. 1999.

[11] K. S. Woo, P. Chook, Y. I. Lolin, A. S. Cheung, L. T. Chan, Y. Y. Sun, J. E. Sanderson, C. Metreweli, and D. S. Celermajer, "Hyperhomocyst(e)inemia is a risk factor for arterial endothelial dysfunction in humans," *Circulation*, vol. 96, no. 8, pp. 2542–2544, Oct. 21, 1997.

[12] K. E. Sorensen, D. S. Celermajer, D. J. Spiegelhalter, D. Georgakopoulus, J. Robinson, O. Thomas, and J. E. Deanfield, "Non-invasive measurement of human endothelium dependent arterial responses: accuracy and reproducibility," *Br. Heart J.*, vol. 74, no. 3, pp. 247–253, Sep. 1995.

[13] J. M. Meinders and A. P. Hoeks, "Simultaneous assessment of diameter and pressure waveforms in the carotid artery," *Ultrasound Med. Biol.*, vol. 30, no. 2, pp. 147–154, Feb. 2004.

[14] M. J. Budoff, F. Flores, J. Tsai, T. Frandsen, H. Yamamoto, and J. Takasu, "Measures of brachial artery distensibility in relation to coronary calcification," *Amer. J. Hypertension*, vol. 16, no. 5, pt. 1, pp. 350–355, May 2003.

[15] E. M. Urbina, T. J. Brinton, A. Elkasabany, and G. S. Berenson, "Brachial artery distensibility and relation to cardiovascular risk factors in healthy young adults (The Bogalusa Heart Study)," *Amer. J. Cardiol.*, vol. 89, no. 8, pp. 946–951, Apr. 15, 2002.

[16] L. Fan, P. Santago, H. Jiang, and D. M. Herrington, "Ultrasound measurement of brachial flow-mediated vasodilator response," *IEEE Trans. Med. Imag.*, vol. 19, no. 6, pp. 621–631, Jun. 2000.

[17] F. Beux, S. Carmassi, M. V. Salvetti, L. Ghiadoni, Y. Huang, S. Taddei, and A. Solvetti, "Automatic evaluation of artery diameter variation from vascular echographics images," *Ultrasound Med. Biol.*, vol. 27, no. 12, pp. 1621–1629, Dec. 2001.

[18] R. J. Woodman, D. A. Playford, G. F. Watts, C. Cheetham, C. Reed, R. R. Taylor, I. B. Puddey, L. J. Beilin, V. Burke, T. A. Mori, and D. Green, "Improved analysis of brachial artery ultrasound using a novel edge-detection software system," *J. Appl. Physiol.*, vol. 91, no. 2, pp. 929–937, Aug. 2001.

[19] M. Sonka, W. Liang, and R. M. Lauer, "Automated analysis of brachial ultrasound image sequences: early detection of cardiovascular disease via surrogates of endothelial function," *IEEE Trans. Med. Imag.*, vol. 21, no. 10, pp. 1271–1279, Oct. 2002.

[20] F. Frangi, M. Laclaustra, and P. Lamata, "A registration-based approach to quantify flow-mediated dilation (FMD) of the brachial artery in ultrasound image sequences," *IEEE Trans. Med. Imag.*, vol. 22, no. 11, pp. 1458–1469, Nov. 2003.

[21] V. R. Newey and D. K. Nassiri, "Online artery diameter measurement in ultrasound images using artificial neural networks," *Ultrasound Med. Biol.*, vol. 28, no. 2, pp. 209–216, Feb. 2002.

[22] A. P. Hoeks, P. J. Brands, F. A. Smeets, and R. S. Reneman, "Assessment of the distensibility of superficial arteries," *Ultrasound Med. Biol.*, vol. 16, no. 2, pp. 121–128, 1990.

[23] G. Bambi, T. Morganti, S. Ricci, E. Boni, F. Guidi, C. Palombo, and P. Tortoli, "A novel ultrasound instrument for investigation of arterial mechanics," *Ultrasonics*, vol. 42, pp. 731–737, Apr. 2004.

[24] K. M. Hiltawsky, A. Wiegratz, M. D. Enderle, and H. Ermert, "Real-time detection of vessel diameters with ultrasound," *Biomedicine Technik*, vol. 48, no. 5, pp. 141–146, May 2003.

[25] V. Gemignani, M. Paterni, A. Benassi, and M. Demi, "Real time contour tracking with a new edge detector," *Real-Time Imag.*, vol. 10, no. 2, pp. 103–116, Apr. 2004.

[26] R. M. Andrei, "A comparison between two edge detectors for a subpixel measurement of the diameter of the brachial artery in ultrasound images" M.S. thesis, Faculty Math, Phys. Natural Sci., Pisa Univ., Pisa, Italy, 2005 [Online]. Available: http://www.ifc.cnr.it/cv

[27] R. S. Reneman, J. M. Meinders, and A. P. Hoeks, "Non-invasive ultrasound in arterial wall dynamics in humans: What have we learned and what remains to be solved," *Eur. Heart J.*, vol. 26, no. 10, pp. 960–966, Mar. 2005.

[28] V. Gemignani, F. Faita, M. Giannoni, and A. Benassi, "A DSP-based platform for rapid prototyping of real time image processing systems," in *Proc. 3rd Int. Symp. Image Signal Process. Anal.*, 2003, vol. 2, pp. 936–939.

[29] V. Gemignani, M. Demi, M. Paterni, M. Giannoni, and A. Benassi, "DSP implementation of real time edge detectors," in *Proc. Speech, Signal Image Process.*, 2001, pp. 1721–1725.

[30] J. A. Jensen, "Field: A program for simulating ultrasound systems," *Med. Biol. Eng. Comput.*, vol. 34, no. 1, pt. 1, pp. 351–353, 1996.

[31] J. A. Jensen and P. Munk, "Computer phantoms for simulating ultrasound B-mode and cfm images," in *Proc. 23rd Acoust. Imag. Symp.*, 1997.

[32] J. M. Bland and D. G. Altman, "Statistical methods for assessing agreement between two methods of clinical measurement," *Lancet*, vol. 1, no. 8476, pp. 307–310.

[33] M. J. Jarvisalo, L. Jartti, J. O. Toikka, J. J. Hartiala, T. Ronnemaa, and O. T. Raitakari, "Noninvasive assessment of brachial artery endothelial function with digital ultrasound and 13-MHz scanning frequency: Feasibility of measuring the true inner luminal diameter using the intima-lumen interface," *Ultrasound Med. Bio.*, vol. 26, no. 8, pp. 1257–1260, Oct. 2000.